Title

Competitive removal of Pb2+ and malachite green from water by magnetic phosphate nanocomposites

Authors

Zhang, Fan
Tang, Xiaoxiu
Huang, Yuxiong
et al.

Publication Date

2019-03-01

DOI

10.1016/j.watres.2018.11.057

Peer reviewed

Water Research 150 (2019) 442–451

Contents lists available at ScienceDirect

Water Research

journal homepage: www.elsevier.com/locate/watres

Competitive removal of Pb^{2+} and malachite green from water by magnetic phosphate nanocomposites

Fan Zhang [a, *, 1], Xiaoxiu Tang [a, 1], Yuxiong Huang [b], Arturo A. Keller [b], Jing Lan [c]

[a] College of Science, Nanjing Agricultural University, Nanjing, 210095, China
[b] Bren School of Environmental Science and Management, University of California, Santa Barbara, CA, 93106, USA
[c] College of Chemistry and Pharmaceutical Sciences, Qingdao Agricultural University, Qingdao, 266109, China

ARTICLE INFO

Article history:
Received 10 August 2018
Received in revised form
18 November 2018
Accepted 19 November 2018
Available online 28 November 2018

Keywords:
Magnetic phosphate nanocomposites
Selective removal
Simultaneous removal
Mechanism
Water treatment

ABSTRACT

The competitive removal of Pb^{2+} and malachite green (MG) from water by three magnetic phosphate nanocomposites ($Fe_3O_4/Ba_3(PO_4)_2$, $Fe_3O_4/Sr_5(PO_4)_3(OH)$, and $Fe_3O_4/Sr_{5x}Ba_{3x}(PO_4)_3(OH)$, namely "FBP", "FSP", and "FSBP", respectively) was systematically investigated compared with Fe_3O_4 ("F") nanoparticle. Temperature and adsorbent dosage for competitive removal were optimized to be 20 °C and 0.05 g in 50 mL. The kinetic and isothermal adsorption results were fitted well with the pseudo-second-order model and Langmuir model, respectively. In the competitive removal process, FSP showed a high affinity to Pb^{2+} (202.8 mg/g) while FBP possessed high selectivity for MG (175.4 mg/g), and FSBP was effective at simultaneous removal of Pb^{2+} and MG, with a capacity of 143.7 and 90.9 mg/g, respectively. The magnetic contents in nanocomposites allow magnetic separation of materials from the water after treatment. We proposed that the simultaneous removal mechanism by FSBP was due to ion exchange between Pb^{2+} and Sr^{2+} in the lattice and then the formation of hydrogen bonds between PO_4^{3-} outside the material's surface and positively charged hydrogen in MG. This study indicates the potential of these phosphate nanocomposites to be used as effective materials for selective or simultaneous removal of Pb^{2+} and MG from water.

1. Introduction

With the rapid development of industrialization, large amounts of heavy metal ions and organic dyes have been released into water systems (Lian et al., 2013). These contaminants are highly toxic, posing a significant threat to aquatic life and human beings (Jia et al., 2015).

As one of the most toxic heavy metals, Pb^{2+} contamination always arouses public concern (Song et al., 2018). Different nanostructured materials have been widely reported for removing Pb^{2+} from aqueous solutions, including grafted and crosslinked chitosan nanoparticles (Ge et al., 2016), 2-hydroxyethylammonium sulfonate immobilized on gamma-Fe_2O_3 nanoparticles (Khani et al., 2016), $Co^{+2}Mo^{+6}$ LDH (Mostafa et al., 2016), metal–organic framework-derived nanoporous adsorbents of $ZnO/ZnFe_2O_4/C$ (Chen et al., 2016), $Mg(OH)_2$ supported nanoscale zero valent iron (Liu et al., 2015), and functionalized carboxylate ferroxane nanoparticles (Moattari et al., 2015). However, the materials for Pb^{2+} removal from metallurgy/electroplating wastewater which usually has lower pH values were still insufficient.

Water contamination by malachite green (MG), a commonly used cationic dye, is attracting increasing attention (Sun et al., 2015). Limited types of nanomaterials have been reported for MG removal, such as a magnetic reduced graphene oxide/zeolitic imidazolate framework self-assembled nanocomposite (Lin and Lee, 2016), cuprous iodide-cupric oxide nano-composite loaded on activated carbon (Nekouei et al., 2016), ZnS:Cu-NP-AC (activated carbon) (Dastkhoon et al., 2015), sodium dodecyl sulfate modified gamma-Al_2O_3 nanoparticles (Mohammadifar et al., 2015), and nano-iron oxide-loaded alginate microspheres (Soni et al., 2014).

The nanomaterials mentioned above have shown promising potential for removal of Pb^{2+} or MG from wastewater individually. However, there is a need for nanomaterials that can simultaneously remove metals and organic dies, such as Pb^{2+} and MG, from aquatic systems (Wang and Ariyanto, 2007; Zhang et al., 2018). This could happen with mixed industrial wastes from electroplating and textile discharges. It should be noted that the co-existence of

* Corresponding author.
E-mail address: zhangfan0128@njau.edu.cn (F. Zhang).
[1] These authors contributed equally.

https://doi.org/10.1016/j.watres.2018.11.057
0043-1354/

different pollutants is considered to be one of the most dangerous sources of environmental pollution (Deng et al., 2013), and multi-component removal studies are useful to identify the competitive performance of several pollutants and play an important role for the proper design and operation of water purification processes (Dil et al., 2017; Sharifpour et al., 2018). When two or more pollutants are present in solution, the removal efficiency of particular contaminant may increase or decrease or remain unchanged. (Dil et al., 2017). Therefore, it is significant to understand the underlying mechanisms and predict the removal efficiency for other pollutants.

In our previous work, we prepared strontium phosphate hybrid nanorod ($Sr_5(PO_4)_3(OH)$ and $SrHPO_4$) by a simple one-pot hydrothermal method. The competitive removal of Pb^{2+} and MG from water by this material was also studied in detail (Zhang et al., 2017). However, it was difficult to separate these strontium phosphate nanorods from solution after treatment resulting in the potential risk of secondary pollution, from residual strontium phosphate hybrid nanorods left after treatment. Hence, the objective of the current study is to investigate the competitive removal of Pb^{2+} and MG by magnetic phosphate nanocomposites, $Fe_3O_4/Sr_5(PO_4)_3(OH)$ (henceforth "FSP") as well as two other materials, $Fe_3O_4/Ba_3(PO_4)_2$ and $Fe_3O_4/Sr_{5x}Ba_{3x}(PO_4)_3(OH)$ ("FBP" and "FSBP", respectively). For comparison, the removal efficiency of Pb^{2+} and MG by pure Fe_3O_4 ("F") nano-crystalline clusters was also evaluated, since these clusters are at the core of FSP, FBP and FSBP. The effects of temperature and adsorbent dosage on the competitive removal were studied. The kinetics and thermodynamics for competitive removal were systematically analyzed by several models. Importantly, the competitive removal mechanism for selective or dual removal of Pb^{2+} and MG by these materials were elucidated which make it a significant study for multifunctional materials in treatment of water with complex contamination.

2. Experimental

2.1. Chemicals

Ferric chloride ($FeCl_3 \cdot 6H_2O$), ethylene glycol (EG), sodium acetate, polyethylene glycol 2000 (PEG2000), strontium nitrate, barium nitrate, cetyltrimethyl ammonium bromide (CTAB), lead nitrate, sodium phosphate, sodium nitrate, sodium sulfate, sodium chloride, nitric acid, sodium hydroxide, and malachite green (MG) were all purchased from Shanghai Sinopharm Chemical Reagent Co., Ltd. (China). CTAB and sodium phosphate were used as versatile soft template and precipitant, respectively. All chemicals and reagents were of analytical grade and used as received without any further purification. The chemical structure of MG is shown in Fig. S1.

2.2. Preparation of materials

The F spherical nano-crystalline clusters (100–500 nm) were prepared using a solvothermal method: Firstly, 1.35 g $FeCl_3 \cdot 6H_2O$ was dissolved in 40 mL EG to form an orange solution. Subsequently, NaAc (3.6 g) and PEG2000 (1 g) were added, followed by vigorously stirring for 30 min. Afterward, the mixture was sealed in a Teflon-lined stainless steel autoclave and maintained at 180 °C for 8 h before cooling to room temperature. Finally, the black powder was rinsed with ethanol several times and dried in a vacuum oven at 60 °C for 6 h. Briefly, the FBP/FSP/FSBP composites were prepared by mixing 1.96 g barium nitrate/1.59 g strontium nitrate/0.98 g barium nitrate and 0.79 g strontium nitrate, respectively, with 0.06 g F spherical clusters and 0.01 g CTAB in 40 mL of deionized (DI) water under stirring to form Solution 1. Solution 2 was prepared by adding 0.82 g sodium phosphate into 10 mL of DI water at 40 °C with continuous stirring for 30 min. Solution 2 was slowly poured into Solution 1 with continuous stirring for 30 min. The mixed solution was transferred into a 100 mL Teflon bottle held in a stainless steel autoclave reactor, sealed, and maintained at 180 °C for 8 h. As the autoclave cooled to room temperature, the powder was washed with DI water and then with ethanol five times. Finally, the samples were dried in a vacuum oven at 60 °C for 4 h, and the yield was ~1.3 g with a yield ratio of ~85%. The resulting magnetic content of F in FBP/FSP/FSBP was calculated to be around 4.6 wt%.

2.3. Batch experiments

Since no obvious interferences were observed in the UV spectrum of MG and Pb^{2+} (Fig. S2), a mixed solution of Pb^{2+} and MG with initial concentration at 500 mg/L (each) was prepared in DI water. The mixed solution pH was adjusted to 5.0 by 0.01 M HNO_3 to avoid the hydrolysis or precipitation of Pb^{2+}.

Batch experiments for removing Pb^{2+} and MG were carried out in beaker with a capacity of 100 mL under mechanic stirring at 200 rpm. Generally, 0.05 g FSP/FBP/FSBP/F, was mixed into 50 mL solution containing Pb^{2+} and MG with initial concentrations at 500 mg/L (each), with mechanic stirring for 60 min at 20 °C and pH 5.0. At predetermined time intervals (0–120 min), 1 mL of the suspension was sampled, then filtered with a 0.45 μm membrane, diluted, following by analysis using inductively coupled plasma-atomic emission spectrometry (ICPAES, Optima 2100, PerkinElmer, USA) and UV–vis spectrophotometer (Shimadzu, model UV1700, Japan) to determine the concentration of Pb^{2+} and MG, respectively. All tests were repeated three times and the mean results used for further analysis.

The removal capacities for Pb^{2+} and MG are calculated as follows (Mostafa et al., 2016):

$$q_e = \frac{(C_0 - C_e)V}{WM} \quad (1)$$

where q_e is the removal capacity at equilibrium (mmol/g); C_0 and C_e are the initial and equilibrium concentrations of Pb^{2+} or MG (mg/L), respectively; V is the volume of solutions (L); W is the dosage of FSP/FBP/FSBP/F used (g); and M is the molecular weight of Pb^{2+} or MG (g/mol).

2.4. Characterization

Morphology of the obtained materials were studied on a Hitachi Limited (model S-4800, Japan) field emission scanning electron microscope (SEM) with energy dispersive spectroscopy (EDS). X-ray diffraction (XRD) patterns were obtained on a Bruker (model AXS D8, Germany) advance X-ray diffract meter with Cu Kα radiation, $\lambda = 0.15406$ nm. The Brunauer-Emmett-Teller (BET) method was applied to obtain the specific surface area of materials with an ASAP 2020 M Micromeritics at 100 °C. The functional groups on the materials were examined via Fourier-transform infrared spectroscopy (FT-IR, Nicolet6700, Thermo, USA). X-ray photoelectron spectroscopy (XPS) was performed on an AXIS UTLTRADLD instrument (Japan). All XPS spectra were calibrated using the binding energy (BE) of C 1*s* (284.8 eV) as the reference.

3. Results and discussion

3.1. Effects of temperature and dosage

As shown in Fig. 1a and b for the competitive removal of Pb^{2+} and MG, there was a slight increase in Pb^{2+} removal by FSP/FSBP/F

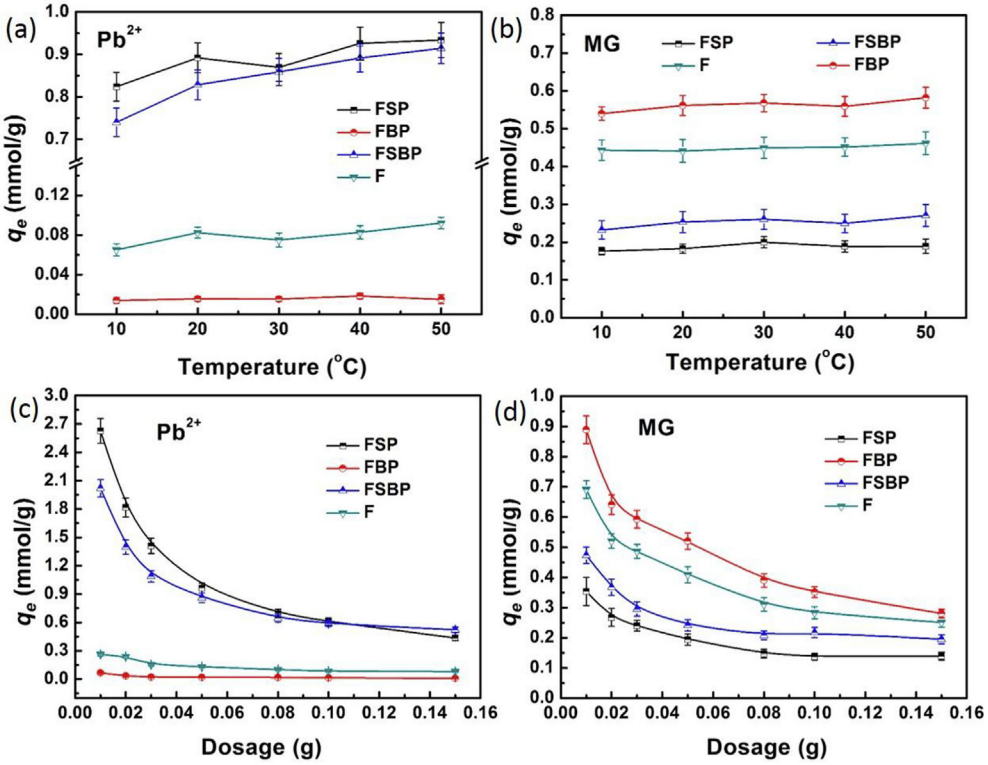

Fig. 1. Competitive removal capacity of Pb^{2+} and MG ($C_0(Pb^{2+}) = C_0(MG) = 500$ mg/L, 20 °C, 60 min) from water (50 mL, pH 5.0) by 0.05 g FSP, FBP, FSBP, and F (a, b) at different temperature and (c, d) with different dosages.

as temperature increased from 10 to 50 °C, while a negligible change was observed for MG removal by all the materials. This indicates that the removal process of Pb^{2+} and MG from mixture is not completely thermodynamically controlled, but kinetically controlled (Zhang et al., 2012). Therefore, no specific temperature control is needed to enhance the removal process, which is beneficial regarding to the operation cost. FSP possessed a high affinity to Pb^{2+} from mixture as it exhibited the highest removal capacity for Pb^{2+} (~0.85 mmol/g) and lowest for MG (~0.18 mmol/g). FBP showed a negligible removal ability of Pb^{2+}, but the highest capacity for MG (~0.55 mmol/g), implying a high selectivity of MG from mixture. FSBP showed high capacity for both Pb^{2+} (0.86 mmol/g) and MG (0.25 mmol/g) at 30 °C, indicating the potential application in mixed contaminated wastewater clean-up. The as-prepared F showed a high removal capacity for MG (~0.45 mmol/g), but low removal capacity for Pb^{2+} (~0.08 mmol/g). The existence of F in FSP, FBP, and FSBP contributed to the removal of MG from the mixture to some extent.

In order to better understand the removal thermodynamic, several thermodynamic parameters which are related to temperature were studied. The values of $\Delta H°$, $\Delta G°$ and $\Delta S°$ were calculated from the following equations and are tabulated in Table 1 (Zare et al., 2018):

$$K_d = q_e/C_e \quad (2)$$

$$\Delta G^{\circ} = -RTLnK_d \quad (3)$$

$$LnK_d = (\Delta S^{\circ}/R) - (\Delta H^{\circ}/RT) \quad (4)$$

Where K_d is the distribution coefficient (mL/g), R is the universal gas constant (8.314 J/mol K), T is absolute temperature (K). $\Delta H°$ (J/mol) and $\Delta S°$ (J/mol K) are enthalpy and entropy changes, respectively. The values of $\Delta H°$ and $\Delta S°$ were calculated from the slope and intercept of the linear plot of ln K_d vs. $1/T$ as showed in Fig. S3.

The negative $\Delta G°$ values for both Pb^{2+} and MG indicate that the adsorption process is thermodynamically spontaneous. With an increase in temperature (Table 1), the absolute value of $\Delta G°$ for all these materials increases slowly, indicating that the adsorption process is more favorable at higher temperature. The positive $\Delta H°$ values approve the endothermic nature of the adsorption process. The positive values of $\Delta S°$ indicate an increase in the randomness at the adsorbent and adsorbate interface, which reveals a good affinity of all these materials towards Pb^{2+} and MG. Similar results were also found in other materials (Gao et al., 2013; Zare et al., 2018).

As shown in Fig. 1c and d, the removal capacity rapidly decreased with increasing adsorbent dosage and then the trend slowed down when dosage was above 0.05 g, which was similar to other reports (Adeogun and Babu, 2015; Jiang et al., 2016; You et al., 2018). Compared to the individual removal of Pb^{2+} or MG at the dosage of 0.01 g (Fig. S4), the removal capacities for Pb^{2+} from the mixture decreased slightly by 5.5% for FSP, 11.1% for FSBP, 0% for both F and FBP, but the removal capacities for MG from the mixture decreased obviously by 18.2% for FBP, 28.6% for F, 31.4% for FSBP, and 20% for FSP. This indicated that there was a competitive sorption between Pb^{2+} and MG, and limited number of reactive sites on the surface of the materials had a greater influence in the removal of MG.

3.2. Adsorption kinetics

Removal efficiency of Pb^{2+} and MG from the mixture increased gradually with a longer exposure time, and equilibrium was reached within 60 min (Fig. S5). Hence, the exposure time of the subsequent experiments were set to be 60 min. Notably, compared

Table 1
Thermodynamic parameters for removing Pb^{2+} and MG from mixture by FSP, FBP, FSBP, and F.

	Material	ΔG°(kJ/mol)					ΔH°(kJ/mol)	ΔS°(J/mol K)
		283 K	293 K	303 K	313 K	323 K		
Pb^{2+}	FSP	−14.71 ± 0.19	−15.53 ± 0.18	−15.96 ± 0.14	−16.74 ± 0.17	−17.32 ± 0.23	3.47 ± 0.12	64.43 ± 0.16
	FBP	−4.16 ± 0.03	−4.55 ± 0.04	−4.68 ± 0.05	−4.94 ± 0.06	−5.31 ± 0.06	2.53 ± 0.08	23.94 ± 0.06
	FSBP	−14.33 ± 0.08	−15.25 ± 0.17	−15.91 ± 0.19	−16.58 ± 0.12	−17.22 ± 0.20	5.81 ± 0.07	71.50 ± 0.11
	F	−7.82 ± 0.06	−8.69 ± 0.07	−8.74 ± 0.08	−9.29 ± 0.06	−9.89 ± 0.09	5.51 ± 0.10	47.56 ± 0.07
MG	FSP	−11.75 ± 0.06	−12.27 ± 0.05	−12.95 ± 0.06	−13.20 ± 0.05	−13.63 ± 0.05	1.61 ± 0.04	47.39 ± 0.06
	FBP	−14.52 ± 0.12	−15.01 ± 0.19	−15.59 ± 0.11	−16.13 ± 0.23	−16.73 ± 0.18	1.14 ± 0.09	55.20 ± 0.08
	FSBP	−12.51 ± 0.11	−13.21 ± 0.09	−13.75 ± 0.13	−14.07 ± 0.12	−14.78 ± 0.10	2.73 ± 0.12	54.12 ± 0.09
	F	−15.24 ± 0.14	−15.94 ± 0.16	−16.53 ± 0.25	−17.01 ± 0.21	−17.74 ± 0.26	1.89 ± 0.15	60.69 ± 0.23

with individual removal of Pb^{2+} or MG (Fig. S6), the decrease on removal capacity of Pb^{2+} in competitive removal was less than that of MG by FSP and FSBP, especially FSP. The differences were smaller when higher dosage was applied, since there would be more available sites for competitive removal (Huang et al., 2016).

In order to further study the kinetics of competitive removal of Pb^{2+} and MG from mixture by these materials, three kinetic models were considered (Figs. 2 and S6): pseudo-first-order, pseudo-second-order, and intra-particle diffusion models. FBP was not included in the subsequent analysis for Pb^{2+} removal due to its negligible Pb^{2+} removal capacity.

Pseudo-first-order kinetic equation (Lee et al., 2011):

$$\ln(q_e - q_t) = \ln q_e - k_1 t \tag{5}$$

where k_1 is the constant rate (g/(mg min)), q_e (mg/g) is the adsorption capacity at equilibrium, and q_t (mg/g) is the adsorption amount at time t (min).

Pseudo-second-order kinetic model(Xiao et al., 2018):

$$\frac{t}{q_t} = \frac{1}{k_2 q_e^2} + \frac{t}{q_e} \tag{6}$$

where k_2 (g/(mg min)) is the constant rate.

Intra-particle diffusion model (Beltrame et al., 2018):

$$q_t = k_{id} t^{0.5} + C \tag{7}$$

where k_{id} (mg/(g $min^{0.5}$)) is the rate constant, and C (mg/g) is intercept which reflects the boundary layer thickness.

For the removal of Pb^{2+} from the mixture by FSP, FSBP, and F, the pseudo-second-order kinetic model fitted the data better (Fig. 2a) than the pseudo-first-order model (Fig. S7a). It suggests that the interaction between Pb^{2+} and the nanocomposites was the rate-limiting step (Yan et al., 2011). The calculated Pb^{2+} adsorption capacity from the pseudo-second-order model by FSP, FSBP, and F was 202.84 mg/g (0.98 mmol/g), 143.68 mg/g (0.69 mmol/g), and 23.65 mg/g (0.11 mmol/g), respectively (Table 2), which was similar to the experimental results. FSBP showed the highest kinetic constant, k_2, among these materials (Table 2). The increased surface energy resulting from structure deformation and structure periodicity reduction when the Sr sites in the lattice are replaced by Ba with a different atomic size (Li et al., 2015) may contribute to the higher capacity. During the competitive removal process, Pb^{2+} ions likely first occupy the available active sites on the surface of FSBP and then are immobilized via the ion-exchange between Pb^{2+} and Sr^{2+}.

For the competitive removal of MG from the mixture (Fig. 2b and Table 3), the kinetic data by all the materials agreed better with the pseudo-second-order model ($R^2 > 0.999$) than the pseudo-first-order model (Fig. S7b). The calculated competitive removal capacity of MG based on the pseudo-second-order model was 208.33 mg/g (0.57 mmol/g) for FBP, 175.44 mg/g (0.48 mmol/g) for F, 90.91 mg/g (0.25 mmol/g) for FSBP, and 65.15 mg/g (0.18 mmol/g) for FSP. This implies that the Ba sites in the phosphate materials are primarily responsible for organic dye removal. Based on these results, FSBP showed good capability to simultaneously remove Pb^{2+} and MG from water. The higher removal capacity and kinetic constant k_2 for Pb^{2+} than that for MG removed by FSBP (Tables 2 and 3) indicates faster approach of Pb^{2+} to occupy the available active sites on the surface of FSBP.

Multiple stages were observed in the plots of q_t versus $t^{0.5}$ for competitive removal of Pb^{2+} and MG (Fig. 2c and d), suggesting that intra-particle diffusion was not the sole rate-limiting step (Huo and Yan, 2012). The $k_{id.1}$, $k_{id.2}$, and $k_{id.3}$ refer to the diffusion rates at different stages during the removal process. The first period ($k_{id.1}$) is the solute transport from the bulk solution to the boundary layer film presented on the adsorbent surface (Reis et al., 2011). The second step ($k_{id.2}$) is the diffusion of solute molecules through the boundary layer film, after which the adsorbates reach the surface of the adsorbent (Reis et al., 2011). The last step ($k_{id.3}$) is intra-particle diffusion when the adsorbates migrate into the porous structure (Wang et al., 2015). As shown in Tables 2 and 3, the kinetic rates for competitive removal of Pb^{2+} and MG by all these materials followed the order of $k_{id.1} > k_{id.2} > k_{id.3}$. With a smaller weight and size compared to MG, Pb^{2+} can transport from the boundary layer film to the material's surface more easily. Therefore, the second stage was shorter for Pb^{2+} removal, compared to MG removal, for FSP and FSBP (Fig. 2). The third step of the removal of Pb^{2+} by FSBP exhibited a longer period than that by FSP and F. This could be explained by two reasons: (a) Pb^{2+} needs to first migrate into material's lattice to initial the ion-exchange between Pb^{2+} with Sr^{2+} while the larger MG molecule only adheres to surface of the material; (b) FSBP possesses a more porous structure (Fig. S8) with the highest BJH adsorption cumulative pore volume (0.78, 0.26, and 0.11 cm^3/g for FSBP, FSP, and FBP, respectively). It should be noted that all the C values referring to the boundary layer thickness were none-zero (Tables 2 and 3), implying that intra-particle diffusion was not the only rate limiting mechanism in the adsorption process (Marrakchi et al., 2017). The increased C values for the three stages were due to the increase of the boundary layer's thickness and the driving force associated with the initial concentrations of Pb^{2+} or MG (Beltrame et al., 2018; Pezoti Jr. et al., 2014).

3.3. Adsorption isotherm

As shown in Fig. S9, all the obtained plots show the 'L' (Langmuir) type adsorption isotherm according to the Giles classification system (Giles et al., 1974), indicating a relatively high affinity between adsorbates and FSP/FBP/FSBP/F (Wan et al., 2010). In the low concentration range, the values of q_e for all materials increased linearly with increased equilibrium concentration (C_e) which may be ascribed to the high driving force provided by high initial

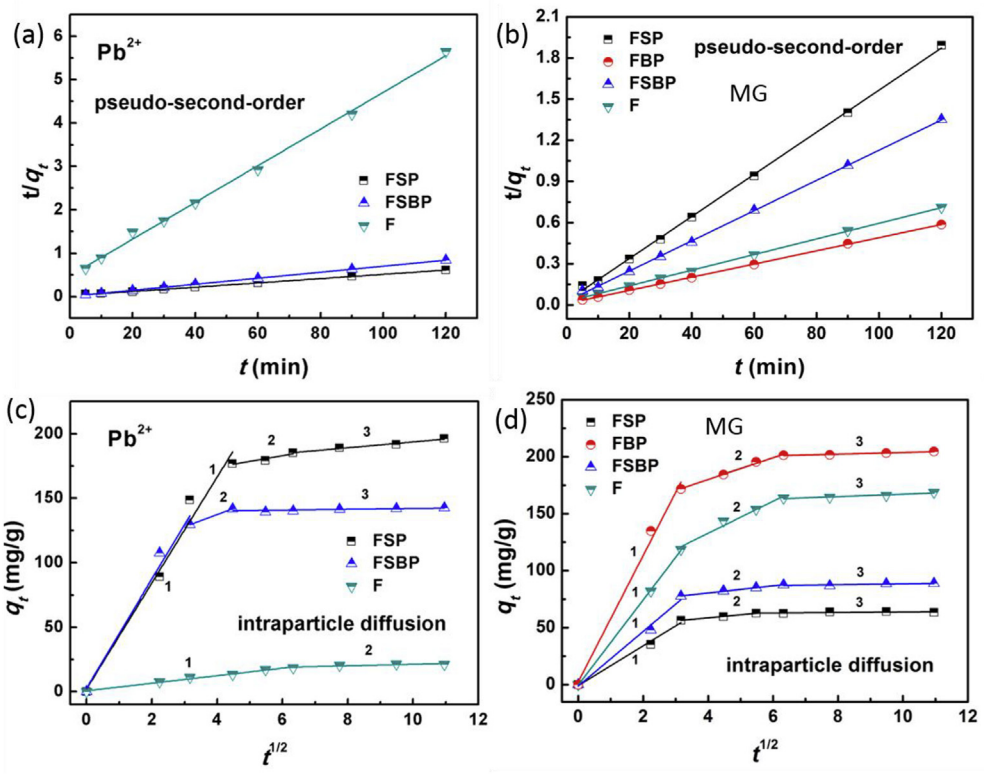

Fig. 2. Kinetics fitted by (a, b) pseudo-second-order model, (c, d) intra-particle diffusion model (curve marked 1, 2, and 3 refer to different adsorption stages) for competitive removal of Pb^{2+} and MG from water by FSP, FBP, FSBP, and F (C_0 (Pb^{2+}) = C_0 (MG) = 500 mg/L, 50 mL, material dosage of 0.05 g, 20 °C, pH 5.0, maintained for 2 h).

Table 2
Kinetic parameters for removing Pb^{2+} from mixture by FSP, FSBP, and F.

Material	pseudo-second-order			intra-particle diffusion								
				k_{id} (mg/(g $min^{0.5}$))			C (mg/g)			R^2		
	k_2 (g/(mg min))	q_e (mg/g)	R^2	$k_{id.1}$	$k_{id.2}$	$k_{id.3}$	C_1	C_2	C_3	R_1^2	R_2^2	R_3^2
FSP	0.0012 ± 0.0003	202.84 ± 2.65	0.9992	41.07 ± 0.38	4.42 ± 0.05	2.26 ± 0.03	2.32 ± 0.02	156.46 ± 2.42	171.02 ± 2.52	0.9688	0.8233	0.9704
FSBP	0.0068 ± 0.0004	143.68 ± 1.46	0.9999	42.27 ± 0.29	9.40 ± 0.03	0.30 ± 0.01	2.96 ± 0.02	99.75 ± 3.26	138.98 ± 2.37	0.9664	–	0.2035
F	0.0037 ± 0.0002	23.65 ± 0.81	0.9969	2.93 ± 0.05	0.57 ± 0.02	–	0.76 ± 0.01	15.51 ± 0.12	–	0.9839	0.6466	–

Table 3
Kinetic parameters for removing MG from mixture by FSP, FBP, FSBP, and F.

Material	pseudo-second-order			intra-particle diffusion								
				k_{id} (mg/(g $min^{0.5}$))			C (mg/g)			R^2		
	k_2 (g/(mg min))	q_e (mg/g)	R^2	$k_{id.1}$	$k_{id.2}$	$k_{id.3}$	C_1	C_2	C_3	R_1^2	R_2^2	R_3^2
FSP	0.0076 ± 0.0008	65.15 ± 1.21	0.9991	17.48 ± 0.15	2.69 ± 0.02	0.21 ± 0.01	−0.86 ± 0.01	47.90 ± 2.11	61.99 ± 1.42	0.9832	0.9923	0.4916
FBP	0.0022 ± 0.0003	208.33 ± 3.73	0.9997	55.41 ± 0.22	9.58 ± 0.03	0.73 ± 0.01	2.49 ± 0.01	141.68 ± 3.21	196.41 ± 3.68	0.9860	0.9920	0.9307
FSBP	0.0044 ± 0.0004	90.91 ± 2.38	0.9994	24.00 ± 0.05	3.09 ± 0.01	0.37 ± 0.01	−1.28 ± 0.01	68.13 ± 1.45	85.54 ± 2.37	0.9802	0.9964	0.9237
F	0.0013 ± 0.0002	175.44 ± 3.47	0.9995	37.35 ± 0.09	14.08 ± 0.11	1.06 ± 0.01	−0.32 ± 0.01	76.48 ± 2.51	156.51 ± 4.43	0.9995	0.9650	0.8893

concentrations to overcome the transfer resistance (Fu et al., 2015). However, the linear growth of the q_e values was retarded at higher C_e range as most of effective sites had been occupied by saturated Pb^{2+} or dye molecules, similar to other reports (Ansari et al., 2017; Hu et al., 2018). In the current study, the q_e values for removal of Pb^{2+} from the mixture followed the order of FSP > FSBP > F > FBP. Higher content of Sr in FSP was beneficial to the effective ion-exchange between Sr^{2+} and Pb^{2+} (Chu et al., 2018; Zhang et al., 2012), leading to the highest removal capacity of Pb^{2+} by FSP. However, the q_e value for removal of MG showed the opposite order: FBP (0.46 mmol/g)> F (0.42 mmol/g)> FSBP (0.26 mmol/g)> FSP (0.17 mmol/g). The highest q_e value of MG by FBP may be ascribed to the effective interaction between Ba and MG (Zhang et al., 2017). The removal of both MG and Pb^{2+} by F may be due to the electrostatic interaction between pollutants and FeOH groups on the surface (Rajput et al., 2016). Therefore, for removal of MG from mixture, the content of these nanomaterials is more crucial to the removal capacity than the surface area of the materials (FSP (58.9 m^2/g)> FSBP (45.3 m^2/g)> F (23.7 m^2/g)> FBP (14.8 m^2/g)).

The Langmuir equation is mainly used for describing monolayer adsorption on the homogeneous surface of adsorbent (Wang et al., 2016). In addition, the binding sites are finite with the same affinity to adsorbate and there is no interaction between adsorbates (Bhattacharyya and Ray, 2014). The equation is as follows:

$$\frac{C_e}{q_e} = \frac{1}{K_L q_m} + \frac{C_e}{q_m} \tag{8}$$

where q_m is the maximum sorption capacity (mg/g), K_L (L/mg) is the Langmuir equilibrium constant. The separation factor (R_L) is a dimensionless parameter that controls the favorability of sorption using the equation (Pourjavadi et al., 2016):

$$R_L = \frac{1}{1 + K_L C_0} \tag{9}$$

where the adsorption can be irreversible ($R_L = 0$), favorable ($0 < R_L < 1$), linear ($R_L = 1$), or unfavorable ($R_L > 1$).

The Freundlich model is to describe multilayer adsorption on heterogeneous surface under various non-ideal conditions (Yazdanbakhsh et al., 2010). This model can be expressed by the following equation:

$$\log q_e = \log K_F + \frac{1}{n} \log C_e \tag{10}$$

where K_F ((mg/g)/(L/mg)$^{-n}$) and n are Freundlich equilibrium constants, which are indicators of the adsorption capacity and distribution, respectively.

Langmiur and Freundlich models were used to further describe the interactive behavior between materials and pollutants (Ma et al., 2015), as shown in Fig. 3a and b. Similarly, FBP was excluded for Pb^{2+} removal due to its negligible removal capacity of Pb^{2+}. The calculated q_m (Tables 4 and 5) for Pb^{2+} and MG from mixture agreed well with the experimental capacities of these materials (Fig. S9). FSP showed the highest q_m for the removal of Pb^{2+} with the lowest R_L and lowest q_m for the removal of MG, yet with the highest R_L from the mixture, implying high affinity to Pb^{2+}. F possessed high q_m for MG removal but low q_m for Pb^{2+} removal. All the $1/n$ values in Tables 4 and 5 were less than one, further implying a favorable removal process. However, the correlation coefficient values (R^2) for Freundlich isotherm for all the materials are a little lower than those of the Langmuir isotherm (Tables 4 and 5), indicating that the adsorption occurs as the monolayer dye adsorbs onto the homogenous material surface (Yazdanbakhsh et al., 2010).

3.4. Mechanism of simultaneous removal

The pristine FSBP are nanorods with a length of ~300 nm (Fig. 4a), while the reclaimed FSBP after treatment have changed their shape to sticky clusters composed of short rods and particles with a smaller size of 50–100 nm (Fig. 4b). The change of shape and size may be due to the existence of pollutants in FSBP which can be supported by the newly found Pb (2.62%) in the reclaimed FSBP (Fig. 4c). Moreover, some small peaks (marked arrows in Fig. 5) in the XRD patterns, which were ascribed to the lead-related phosphate (Chu et al., 2018; Ma et al., 1995), were observed in reclaimed FSBP, confirming the replacement of Sr by Pb in FSBP's lattice. Compared to the pristine F (Fig. 4d), the surface of reclaimed F (Fig. 4e) became fuzzy and sticky which may be also ascribed to the adsorbed pollutants. No obvious change can be found in the XRD patterns of F before and after treatment (Fig. 5), implying that Pb^{2+} ions were immobilized on the surface of F instead of entering into lattice of Fe_3O_4 crystals. As a result, 57% of adsorbed Pb^{2+} ions were found re-leaching from the surface of F into water after 10 h. There

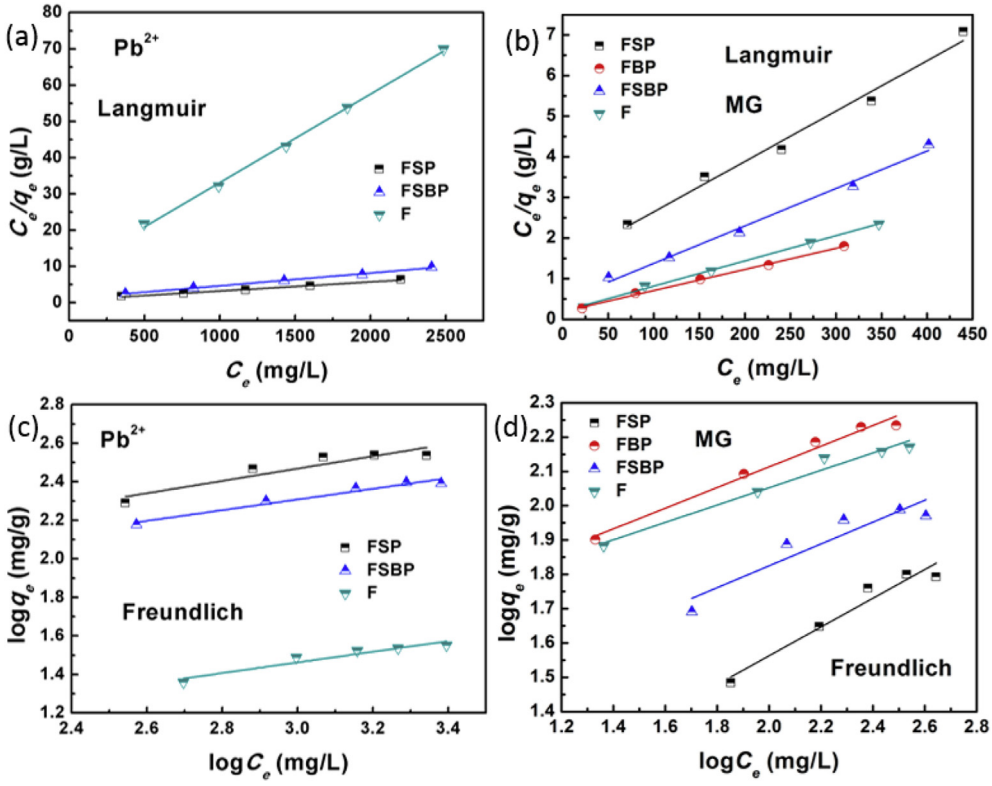

Fig. 3. Fitting plots of competitive removal of Pb^{2+} and MG from mixture: (a, b) Langmiur and (c, d) Freundlich isotherm model onto FSP, FBP, FSBP, and F.

Table 4
Isotherm parameters for removing Pb^{2+} from mixture by FSP, FSBP, and F.

Material	Langmuir				Freundlich		
	q_m (mg/g)	K_L (L/mg)	R_L	R^2	K_F ((mg/g)/(L/mg)$^{-n}$)	1/n	R^2
FSP	401.61 ± 4.58	0.0033 ± 0.0001	0.38 ± 0.01	0.989	32.31 ± 0.09	0.320 ± 0.005	0.839
FSBP	284.09 ± 3.91	0.0030 ± 0.0001	0.40 ± 0.01	0.997	29.93 ± 0.07	0.277 ± 0.005	0.953
F	40.95 ± 1.21	0.0028 ± 0.0001	0.42 ± 0.01	0.998	4.31 ± 0.02	0.276 ± 0.005	0.896

Table 5
Isotherm parameters for removing MG from mixture by FSP, FBP, FSBP, and F.

Material	Langmuir				Freundlich		
	q_m (mg/g)	K_L (L/mg)	R_L	R^2	K_F ((mg/g)/(L/mg)$^{-n}$)	1/n	R^2
FSP	80.65 ± 0.97	0.0088 ± 0.0009	0.19 ± 0.01	0.982	5.30 ± 0.05	0.419 ± 0.025	0.935
FBP	192.31 ± 3.52	0.0276 ± 0.0015	0.07 ± 0.01	0.996	32.45 ± 0.13	0.301 ± 0.008	0.977
FSBP	108.70 ± 2.31	0.0203 ± 0.0011	0.09 ± 0.01	0.989	15.43 ± 0.09	0.318 ± 0.009	0.840
F	161.29 ± 2.56	0.0314 ± 0.0019	0.06 ± 0.01	0.997	35.20 ± 0.15	0.253 ± 0.015	0.966

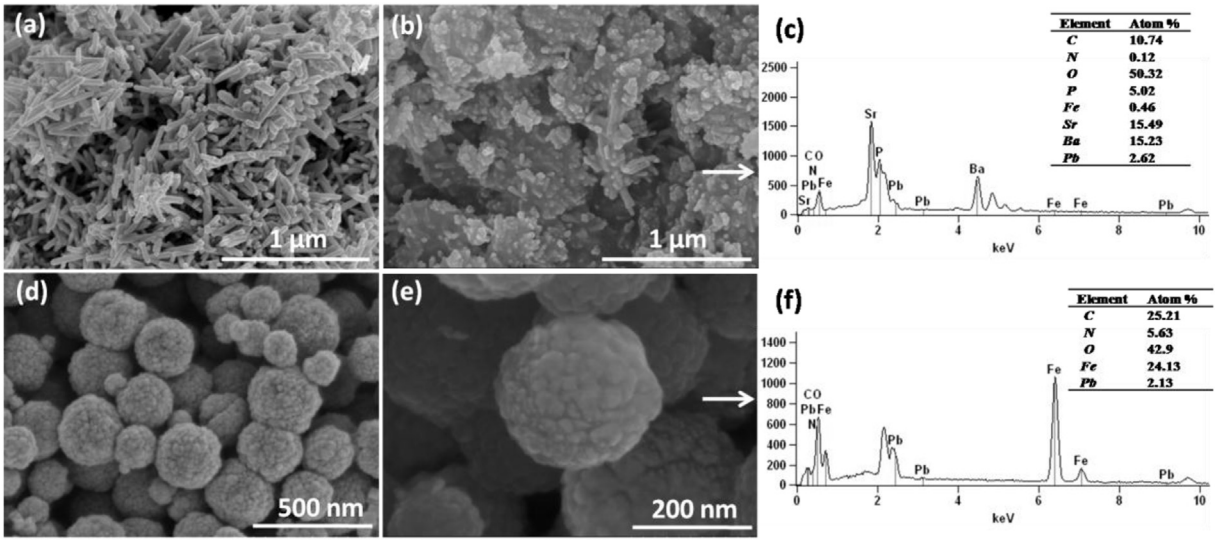

Fig. 4. SEM of pristine (a) FSBP and (d) F; SEM and EDS results of the reclaimed (b, c) FSBP and (e, f) F after simultaneous removal of Pb^{2+} and MG from water (50 mL, C_0 (Pb^{2+}) = C_0 (MG) = 500 mg/L, material dosage of 0.05 g, 20 °C, pH 5.0, maintained for 2 h).

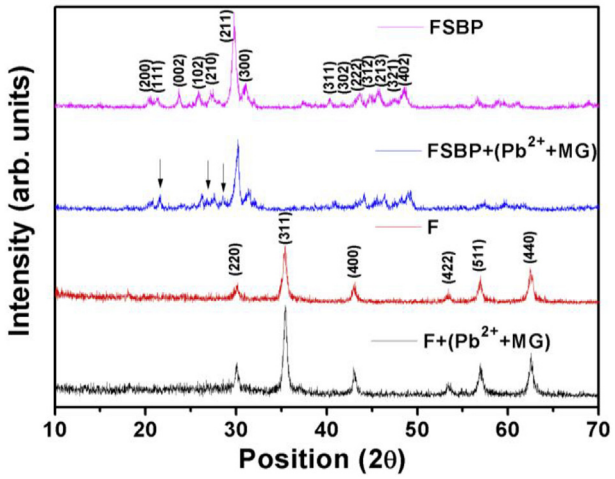

Fig. 5. XRD patterns of FSBP and F before and after simutanous removal application.

is a concern of inducing secondary pollution to the water system as the released Pb^{2+} ions possess a high toxicity to aquatic life and human beings (Song et al., 2018). A higher percentage of N (5.63 at %) in F than that in FSBP (0.12 at%) indicates that more MG can be adsorbed on the surface of F, which agrees well with the removal capacities (Fig. S9). It should be noted that the element leaching of Ba from FBP and FSBP into solution in the removal process was 1.9 and 1.7 mg/L, respectively, which is below the USEPA Maximum Contaminant Level (2.0 mg/L) for Ba in drinking water.

Some of the FT-IR characteristic peaks of MG (marked arrows) were found in the used FSBP, but not in pristine FSBP (Fig. 6), demonstrating the existence of MG in the reclaimed FSBP. The peaks at 1637 cm^{-1}, 1558 cm^{-1}, 1438 cm^{-1}, 1407 cm^{-1}, 1321 cm^{-1}, and 1273 cm^{-1} may be characterized to the vibrations of C=C stretching, N-H bending, benzene ring, C-H bending of methyl, -C-N, and C-N stretching, respectively (Lee et al., 2011; Leng et al., 2015; Sun et al., 2015; Wei et al., 2014). The peaks at 885.2 cm^{-1}, 761.2 cm^{-1}, and 677.9 cm^{-1} can be ascribed to aromatic C–H bending (Wei et al., 2014). They showed obvious shifts compared with pristine MG. In addition, broadening of peaks at 1637 cm^{-1} and 1030 cm^{-1} were observed in used FSBP. These changes of shift

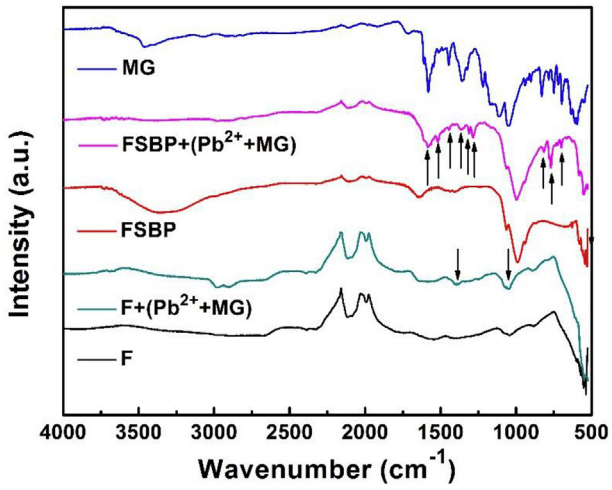

Fig. 6. FT-IR spectra of MG, FSBP, and F before and after simultaneous removal application.

and broadening of peaks suggested the possible chemical interactions (e.g. hydrogen bonding (Ahmed and Jhung, 2017)) between pollutants and FSBP. No obvious change was found in the FT-IR spectra of F before and after treatment (Fig. 6). The peaks at 1350 cm^{-1} and 1047 cm^{-1} can be attributed to C-N stretching and C-H bending, respectively, implying the existence of MG in reclaimed F. It should be noted that even more N was found in the reclaimed F than that in reclaimed FSBP according to EDS results (Fig. 4), but less groups ascribed to MG were found in FT-IR spectrum of reclaimed F (Fig. 6). It suggested that the interaction between F and MG may be weak physical bonding, which was also supported by the fact that after staying in water for 10 h, more leaching of adsorbed MG was found from reclaimed F (42%) than that from reclaimed FSBP (15%). The unstable binding between MG and F would limit its application due to the potential secondary pollution. The phosphate in FSBP played a significant role in the stable immobilization of Pb^{2+} and MG, while the content of F in FSBP was mainly responsible for magnetic separation of FSBP from water after treatment.

As shown in Fig. 7a and b, the newly found Pb peaks (Pb 4*p*, Pb

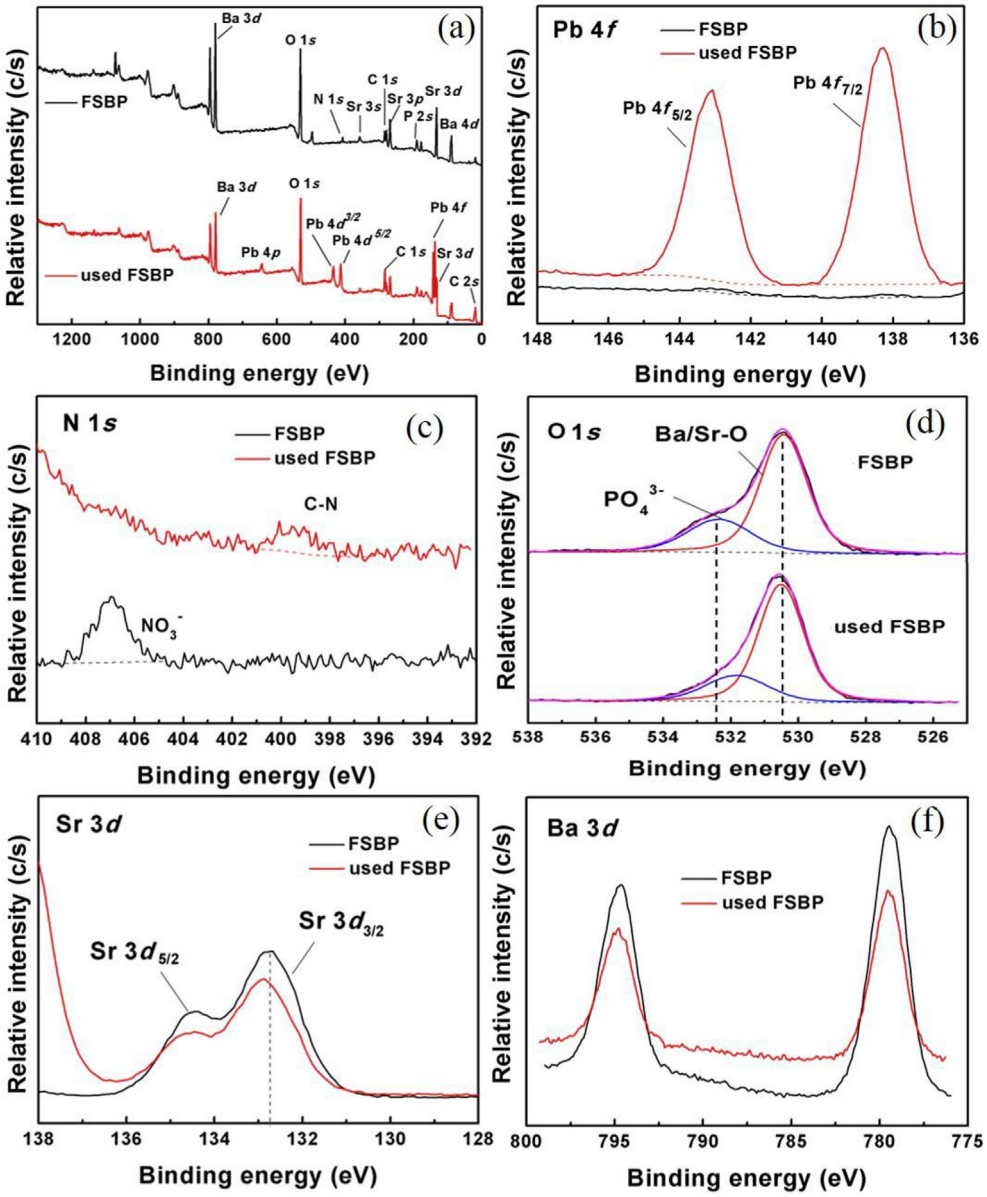

Fig. 7. XPS spectra of (a) survey scan, (b) Pb 4f, (c) O 1s, (d) N 1s, (e) Sr 3d, and (f) Ba 3d for FSBP before and after simultaneous removal application.

4*d*, and Pb 4*f*) and the decreased Sr 3*d* peak signal in XPS spectra demonstrated that Pb^{2+} was immobilized mainly by replacing Sr in the lattice of FSBP. The increased C peaks (C 1*s* and C 2*s*) confirmed the existence of MG in the used FSBP (Fig. 7a). The newly detected N 1*s* peak (Fig. 7c) which can be ascribed to be C-N group in MG showed no obvious shift compared to pristine MG, suggesting that the N containing groups were not responsible for strong bonding which can lead to electron density change (Mashtalir et al., 2014). As shown in Fig. 7d, the high-resolution O 1*s* spectra before and after removal can be deconvoluted into the two peaks as indicated. The peak ascribed to PO_4^{3-} was shifted to the low binding energy, implying a different electron density at oxygen in P–O–Pb/MG linkages compared to P–O–Sr/Ba (Sudarsan et al., 2002). On the other hand, the peak ascribed to Ba/Sr-O showed no obvious shift. Slight shift and peak area decrease were found in Sr 3*d* (Fig. 7e) after application which may be due to the replacement of Sr by Pb in the lattice. The unchanged position of Ba 3*d* spectra (Fig. 7f) implied that the Ba element was not involved in the chemical interaction. Therefore, the mechanism of simultaneously removing Pb^{2+} and MG by FSBP is proposed to be ion exchange between Pb^{2+} and Sr^{2+} in the lattice as well as the hydrogen bonds between PO_4^{3-} on surface of FSBP and positively charged hydrogen group of MG.

4. Conclusions

In this work, the competitive removal of Pb^{2+} and MG from water by three magnetic phosphate nanocomposites (FSP, FBP, and FSBP) was investigated in detail, and compared to the removal of the magnetic iron oxide core (F). Effects of temperature and adsorbent dosage were studied to optimize the removal processes. Kinetic and isothermal were studied with three kinetic models and two isothermal models. FSP and FBP showed a high selectivity of Pb^{2+} and MG from mixture, respectively, while FSBP can effectively remove both Pb^{2+} and MG from mixture. The phosphate in these nanocomposites was mainly responsible for the removal performance, while the magnetic characteristics provided by F enhance the magnetic separation of the pollutant-laden nanocomposites from water after treatment. The mechanism of simultaneous removal by FSBP was proposed to be the ion exchange between Pb^{2+} and Sr^{2+} in the lattice and the hydrogen bonds between PO_4^{3-} on surface of FSBP and positively charged hydrogen group of MG. It demonstrated the promising application of the magnetic phosphate nanocomposites for treating multi-pollutants wastewater.

Declaration of interests

The authors declare that they have no known competing financial interests or personal relationships that could have appeared to influence the work reported in this paper.

The authors declare the following financial interests/personal relationships which may be considered as potential competing interests:

Acknowledgements

This work was financially supported by the Jiangsu Natural Science Foundation of China (Grant No. SBK2017020336), the Fundamental Research Funds for the Central Universities (Grant No. KYZ201747), and the National Natural Science Funds of China (Grant No. 51402153). This work was in part supported by the National Science Foundation and the U.S. Environmental Protection Agency under NSF-EF0830117. Any opinions, findings, conclusions or recommendations expressed in this material are those of the authors do not necessarily reflect the views of the funding agencies.

Appendix A. Supplementary data

Supplementary data to this article can be found online at https://doi.org/10.1016/j.watres.2018.11.057.

References

Adeogun, A.I., Babu, R.B., 2015. One-step synthesized calcium phosphate-based material for the removal of alizarin S dye from aqueous solutions: isothermal, kinetics, and thermodynamics studies. Appl. Nanosci. 1–13.
Ahmed, I., Jhung, S.H., 2017. Applications of metal-organic frameworks in adsorption/separation processes via hydrogen bonding interactions. Chem. Eng. J. 310, 197–215.
Ansari, M.O., Kumar, R., Ansari, S.A., Ansari, S.P., Barakat, M.A., Alshahrie, A., Cho, M.H., 2017. Anion selective pTSA doped polyaniline@graphene oxide-multiwalled carbon nanotube composite for Cr(VI) and Congo red adsorption. J. Colloid Interface Sci. 496, 407–415.
Beltrame, K.K., Cazetta, A.L., de Souza, P.S.C., Spessato, L., Silva, T.L., Almeida, V.C., 2018. Adsorption of caffeine on mesoporous activated carbon fibers prepared from pineapple plant leaves. Ecotoxicol. Environ. Saf. 147, 64–71.
Bhattacharyya, R., Ray, S.K., 2014. Micro- and nano-sized bentonite filled composite superabsorbents of chitosan and acrylic copolymer for removal of synthetic dyes from water. Appl. Clay Sci. 101, 510–520.
Chen, D., Shen, W., Wu, S., Chen, C., Luo, X., Guo, L., 2016. Ion exchange induced removal of Pb(II) by MOF-derived magnetic inorganic sorbents. Nanoscale 8, 7172–7179.
Chu, W., Lu, Z., Tan, R., Tang, S., Xu, W., Song, W., Zhao, J., 2018. Comparative study on Pb2+ removal using hydrothermal synthesized β-SrHPO4, Sr3(PO4)2, and Sr5(PO4)3(OH) powders. Powder Technol. 329, 420–425.
Dastkhoon, M., Ghaedi, M., Asfaram, A., Goudarzi, A., Langroodi, S.M., Tyagi, I., Agarwal, S., Gupta, V.K., 2015. Ultrasound assisted adsorption of malachite green dye onto ZnS:Cu-NP-AC: equilibrium isotherms and kinetic studies - response surface optimization. Separ. Purif. Technol. 156, 780–788.
Deng, J.-H., Zhang, X.-R., Zeng, G.-M., Gong, J.-L., Niu, Q.-Y., Liang, J., 2013. Simultaneous removal of Cd(II) and ionic dyes from aqueous solution using magnetic graphene oxide nanocomposite as an adsorbent. Chem. Eng. J. 226, 189–200.
Dil, E.A., Ghaedi, M., Asfaram, A., Hajati, S., Mehrabi, F., Goudarzi, A., 2017. Preparation of nanomaterials for the ultrasound-enhanced removal of Pb2+ ions and malachite green dye: chemometric optimization and modeling. Ultrason. Sonochem. 34, 677–691.
Fu, J., Chen, Z., Wang, M., Liu, S., Zhang, J., Zhang, J., Han, R., Xu, Q., 2015. Adsorption of methylene blue by a high-efficiency adsorbent (polydopamine microspheres): kinetics, isotherm, thermodynamics and mechanism analysis. Chem. Eng. J. 259, 53–61.
Gao, H.J., Kan, T.T., Zhao, S.Y., Qian, Y.X., Cheng, X.Y., Wu, W.L., Wang, X.D., Zheng, L.G., 2013. Removal of anionic azo dyes from aqueous solution by functional ionic liquid cross-linked polymer. J. Hazard Mater. 261, 83–90.
Ge, H., Hua, T., Chen, X., 2016. Selective adsorption of lead on grafted and cross-linked chitosan nanoparticles prepared by using Pb2+ as template. J. Hazard Mater. 308, 225–232.
Giles, C.H., Smith, D., Huitson, A., 1974. A general treatment and classification of the solute adsorption isotherm. I. Theoretical. J. Colloid Interface Sci. 47, 766–778.
Hu, M., Yan, X., Hu, X., Zhang, J., Feng, R., Zhou, M., 2018. Ultra-high adsorption capacity of MgO/SiO2 composites with rough surfaces for Congo red removal from water. J. Colloid Interface Sci. 510, 111–117.
Huang, Y., Fulton, A.N., Keller, A.A., 2016. Simultaneous removal of PAHs and metal contaminants from water using magnetic nanoparticle adsorbents. Sci. Total Environ. 571, 1029–1036.
Huo, S.-H., Yan, X.-P., 2012. Metal-organic framework MIL-100(Fe) for the adsorption of malachite green from aqueous solution. J. Mater. Chem. 22, 7449–7455.
Jia, Y., Jin, Q., Li, Y., Sun, Y., Huo, J., Zhao, X., 2015. Investigation of the adsorption behaviour of different types of dyes on MIL-100(Fe) and their removal from natural water. Anal. Methods 7, 1463–1470.
Jiang, Y., Gong, J.L., Zeng, G.M., Ou, X.M., Chang, Y.N., Deng, C.H., Zhang, J., Liu, H.Y., Huang, S.Y., 2016. Magnetic chitosan-graphene oxide composite for antimicrobial and dye removal applications. Int. J. Biol. Macromol. 82, 702–710.
Khani, R., Sobhani, S., Beyki, M.H., 2016. Highly selective and efficient removal of lead with magnetic nano-adsorbent: multivariate optimization, isotherm and thermodynamic studies. J. Colloid Interface Sci. 466, 198–205.
Lee, Y.-C., Kim, E.J., Yang, J.-W., Shin, H.-J., 2011. Removal of malachite green by adsorption and precipitation using aminopropyl functionalized magnesium phyllosilicate. J. Hazard Mater. 192, 62–70.
Leng, L., Yuan, X., Zeng, G., Shao, J., Chen, X., Wu, Z., Wang, H., Peng, X., 2015. Surface characterization of rice husk bio-char produced by liquefaction and application for cationic dye (Malachite green) adsorption. Fuel 155, 77–85.
Li, J., Ng, D.H.L., Song, P., Song, Y., Kong, C., 2015. Bio-inspired synthesis and characterization of mesoporous ZnFe2O4 hollow fibers with enhancement of adsorption capacity for acid dye. J. Ind. Eng. Chem. 23, 290–298.
Lian, G., Zhang, X., Si, H., Wang, J., Cui, D., Wang, Q., 2013. Boron nitride ultrathin fibrous nanonets: one-step synthesis and applications for ultrafast adsorption for water treatment and selective filtration of nanoparticles. ACS Appl. Mater. Interfaces 5, 12773–12778.
Lin, K.-Y.A., Lee, W.-D., 2016. Highly efficient removal of Malachite green from water

by a magnetic reduced graphene oxide/zeolitic imidazolate framework self-assembled nanocomposite. Appl. Surf. Sci. 361, 114–121.
Liu, M., Wang, Y., Chen, L., Zhang, Y., Lin, Z., 2015. Mg(OH)(2) supported nanoscale zero valent iron enhancing the removal of Pb(II) from aqueous solution. ACS Appl. Mater. Interfaces 7, 7961–7969.
Ma, Q.Y., Logan, T.J., Traina, S.J., 1995. Lead immobilization from aqueous solutions and contaminated soils using phosphate rocks. Environ. Sci. Technol. 29, 1118–1126.
Ma, S., Zhan, S., Jia, Y., Zhou, Q., 2015. Highly efficient antibacterial and Pb(II) removal effects of Ag-CoFe2O4-GO nanocomposite. ACS Appl. Mater. Interfaces 7, 10576–10586.
Marrakchi, F., Ahmed, M.J., Khanday, W.A., Asif, M., Hameed, B.H., 2017. Mesoporous-activated carbon prepared from chitosan flakes via single-step sodium hydroxide activation for the adsorption of methylene blue. Int. J. Biol. Macromol. 98, 233.
Mashtalir, O., Cook, K.M., Mochalin, V.N., Crowe, M., Barsoum, M.W., Gogotsi, Y., 2014. Dye adsorption and decomposition on two-dimensional titanium carbide in aqueous media. J. Mater. Chem. 2, 14334–14338.
Moattari, R.M., Rahimi, S., Rajabi, L., Derakhshan, A.A., Keyhani, M., 2015. Statistical investigation of lead removal with various functionalized carboxylate ferroxane nanoparticles. J. Hazard Mater. 283, 276–291.
Mohammadifar, E., Shemirani, F., Majidi, B., Ezoddin, M., 2015. Application of modified nano-gamma-alumina as an efficient adsorbent for removing malachite green (MG) from aqueous solution. Desalin. Water Treat. 54, 758–768.
Mostafa, M.S., Bakr, A.-S.A., El Naggar, A.M.A., Sultan, E.-S.A., 2016. Water decontamination via the removal of Pb (II) using a new generation of highly energetic surface nano-material: Co+2Mo+6 LDH. J. Colloid Interface Sci. 461, 261–272.
Nekouei, F., Noorizadeh, H., Nekouei, S., Asif, M., Tyagi, I., Agarwal, S., Gupta, V.K., 2016. Removal of malachite green from aqueous solutions by cuprous iodide-cupric oxide nano-composite loaded on activated carbon as a new sorbent for solid phase extraction: isotherm, kinetics and thermodynamic studies. J. Mol. Liq. 213, 360–368.
Pezoti Jr., O., Cazetta, A.L., Souza, I.P.A.F., Bedin, K.C., Martins, A.C., Silva, T.L., Almeida, V.C., 2014. Adsorption studies of methylene blue onto ZnCl2-activated carbon produced from buriti shells (Mauritia flexuosa L.). J. Ind. Eng. Chem. 20, 4401–4407.
Pourjavadi, A., Abedin-Moghanaki, A., Tavakoli, A., 2016. Efficient removal of cationic dyes using a new magnetic nanocomposite based on starch-g-poly(vinylalcohol) and functionalized with sulfate groups. RSC Adv. 6, 38042–38051.
Rajput, S., Pittman Jr., C.U., Mohan, D., 2016. Magnetic magnetite (Fe3O4) nanoparticle synthesis and applications for lead (Pb2+) and chromium (Cr6+) removal from water. J. Colloid Interface Sci. 468, 334–346.
Reis, L.G.T. Dos, Robaina, N.F., Pacheco, W.F., Cassella, R.J., 2011. Separation of Malachite Green and Methyl Green cationic dyes from aqueous medium by adsorption on Amberlite XAD-2 and XAD-4 resins using sodium dodecylsulfate as Carrier. Chem. Eng. J. 171, 532–540.
Sharifpour, E., Khafri, H.Z., Ghaedi, M., Asfaram, A., Jannesar, R., 2018. Isotherms and kinetic study of ultrasound-assisted adsorption of malachite green and Pb2+ ions from aqueous samples by copper sulfide nanorods loaded on activated carbon: experimental design optimization. Ultrason. Sonochem. 40, 373–382.
Song, M., Wei, Y., Cai, S., Yu, L., Zhong, Z., Jin, B., 2018. Study on adsorption properties and mechanism of Pb^{2+} with different carbon based adsorbents. Sci. Total Environ. 618, 1416–1422.
Soni, A., Tiwari, A., Bajpai, A.K., 2014. Removal of malachite green from aqueous solution using nano-iron oxide-loaded alginate microspheres: batch and column studies. Res. Chem. Intermed. 40, 913–930.
Sudarsan, V., Muthe, K.P., Vyas, J.C., Kulshreshtha, S.K., 2002. PO43- tetrahedra in SbPO4 and SbOPO4: a P-31 NMR and XPS study. J. Alloy. Comp. 336, 119–123.
Sun, L., Hu, S., Sun, H., Guo, H., Zhu, H., Liu, M., Sun, H., 2015. Malachite green adsorption onto Fe_3O_4@SiO_2-NH_2: isotherms, kinetic and process optimization. RSC Adv. 5, 11837–11844.
Wan, S.W.N., Ariff, N.F.M., Hashim, A., Hanafiah, M.A.K.M., 2010. Malachite green adsorption onto chitosan coated bentonite beads: isotherms, kinetics and mechanism. Clean. - Soil, Air, Water 38, 394–400.
Wang, D., Liu, L., Jiang, X., Yu, J., Chen, X., 2015. Adsorption and removal of malachite green from aqueous solution using magnetic beta-cyclodextrin-graphene oxide nanocomposites as adsorbents. Colloid. Surface. Physicochem. Eng. Aspect. 466, 166–173.
Wang, S., Ariyanto, E., 2007. Competitive adsorption of malachite green and Pb ions on natural zeolite. J. Colloid Interface Sci. 314 (1), 25–31.
Wang, Y., Zhang, Y., Hou, C., Liu, M., 2016. Mussel-inspired synthesis of magnetic polydopamine-chitosan nanoparticles as biosorbent for dyes and metals removal. J. Taiwan Inst. Chem. Eng. 61, 292–298.
Wei, A., Liu, B., Zhao, H., Chen, Y., Wang, W., Ma, Y., Yang, H., Liu, S., 2014. Synthesis and formation mechanism of flowerlike architectures assembled from ultrathin NiO nanoflakes and their adsorption to malachite green and acid red in water. Chem. Eng. J. 239, 141–148.
Xiao, Y., Azaiez, J., Hill, J.M., 2018. Erroneous application of pseudo-second-order adsorption kinetics model: ignored assumptions and spurious correlations. Ind. Eng. Chem. Res. 57, 2705–2709.
Yan, H., Zhang, W., Kan, X., Dong, L., Jiang, Z., Li, H., Yang, H., Cheng, R., 2011. Sorption of methylene blue by carboxymethyl cellulose and reuse process in a secondary sorption. Colloid. Surface. Physicochem. Eng. Aspect. 380, 143–151.
Yazdanbakhsh, M., Khosravi, I., Goharshadi, E.K., Youssefi, A., 2010. Fabrication of nanospinel ZnCr2O4 using sol-gel method and its application on removal of azo dye from aqueous solution. J. Hazard Mater. 184, 684–689.
You, L., Huang, C., Lu, F., Wang, A., Liu, X., Zhang, Q., 2018. Facile synthesis of high performance porous magnetic chitosan - polyethylenimine polymer composite for Congo red removal. Int. J. Biol. Macromol. 107, 1620–1628.
Zare, E.N., Lakouraj, M.M., Kasirian, N., 2018. Development of effective nano-biosorbent based on poly m-phenylenediamine grafted dextrin for removal of Pb (II) and methylene blue from water. Carbohydr. Polym. 201, 539–548.
Zhang, F., Wei, Z., Zhang, W., Cui, H., 2017. Effective adsorption of malachite green using magnetic barium phosphate composite from aqueous solution. Spectrochim. Acta Part A-Molecular Biomol. Spectrosc. 182, 116–122.
Zhang, F., Zhao, Z., Tan, R., Xu, W., Jiang, G., Song, W., 2012. Efficient and selective immobilization of Pb2+ in highly acidic wastewater using strontium hydroxyapatite nanorods. Chem. Eng. J. 203, 110–114.
Zhang, X., Lin, Q., Luo, S., Ruan, K., Peng, K., 2018. Preparation of novel oxidized mesoporous carbon with excellent adsorption performance for removal of malachite green and lead ion. Appl. Surf. Sci. 442, 322–331.